Characterization of the Coral Allene Oxide Synthase Active Site with UV−Visible Absorption, Magnetic Circular Dichroism, and Electron Paramagnetic Resonance Spectroscopy: Evidence for Tyrosinate Ligation to the Ferric Enzyme Heme Iron†

Biji D. Abraham,‡ Masanori Sono,‡ Olivier Boutaud,§ Anthony Shriner,|| John H. Dawson,*,‡,⊥ Alan R. Brash,§ and Betty J. Gaffney*,||

Department of Chemistry and Biochemistry and School of Medicine, University of South Carolina, Columbia, South Carolina 29208, Department of Pharmacology, Vanderbilt University Medical Center, Nashville, Tennessee 37232-6602, and Department of Biological Science, Florida State University, Tallahassee, Florida 32306-4380

Received September 8, 2000; Revised Manuscript Received November 21, 2000

ABSTRACT: Coral allene oxide synthase (AOS), a hemoprotein with weak sequence homology to catalase, is the N-terminal domain of a naturally occurring fusion protein with an 8*R*-lipoxygenase. AOS converts 8*R*-hydroperoxyeicosatetraenoic acid to the corresponding allene oxide. The UV−visible absorption and magnetic circular dichroism spectra of ferric AOS and of its cyanide and azide complexes, and the electron paramagnetic resonance spectra of native AOS (high-spin, $g = 6.56, 5.22, 2.00$) and of its cyanide adduct (low-spin, $g = 2.86, 2.24, 1.60$) closely resemble the corresponding spectra of bovine liver catalase (BLC). These results provide strong evidence for tyrosinate ligation to the heme iron of AOS as has been established for catalases. On the other hand, the positive circular dichroism bands in the Soret region for all three derivatives of ferric AOS are almost the mirror image of those in catalase. In addition, the cyanide affinity of native AOS ($K_d = 10$ mM at pH 7) is about 3 orders of magnitude lower than that of BLC. Thus, while these results conclusively support a common tyrosinate-ligated heme in AOS as in catalase, significant differences exist in the interaction between their respective heme prosthetic groups and protein environments, and in the access of small molecules to the heme iron.

Interest in the enzymology underlying the high prostaglandin content of the Caribbean sea whip coral, *Plexaura homomalla*, has been the impetus for several biochemical investigations. Arachidonic acid is metabolized in extracts of *P. homomalla* and related corals by a lipoxygenase (LOX)[1] pathway that appeared initially to relate to the production of cyclopentenone prostaglandins (*1*, *2*). An 8*R*-lipoxygenase converts arachidonic acid to 8*R*-hydroperoxyeicosatetraenoic acid (8R-HPETE), and the fatty acid hydroperoxide is then enzymatically dehydrated to an allene oxide, an epoxide with a propensity to cyclize to cyclopentenone derivatives. Brash et al., in 1997, isolated the cDNA of an 8*R*-lipoxygenase from *P. homomalla* and found it to occur with an extra sequence in the open reading frame that encodes the allene oxide synthase (AOS) (*3*). This natural fusion protein in coral consists of a LOX C-terminal domain (79 kDa) and an AOS N-terminal domain (43 kDa). The truncated (AOS) construct catalyzes an identical reaction to the AOS domain in the fusion protein, converting 8R-HPETE solely to the allene oxide. The truncated construct exhibits very high turnover number (1400/s) (*4*), although, due to the weaker expression of the fusion protein in *E. coli*, the comparable values for the fusion protein remain to be determined.[2] Although allene oxide has not proven to be an intermediate in the prostaglandin synthesis pathway (*5*), it may be linked to prostanoid type products such as clavulones and punaglandins of other corals (*2*, *6*, *7*). Allene oxides are very unstable epoxides; they readily hydrolyze into ketols, cyclopentenones, and other rearrangement products (*8*−*10*).

The production of allene oxides from fatty acid hydroperoxides also occurs in plants. In flaxseed and other plants, AOS is a cytochrome P450, now designated as the subfamily CYP74A (*11*, *12*). This ∼55 kDa enzyme plays a key role in the conversion of linolenic acid to jasmonic acid, a plant

† This research was supported by National Institutes of Health Grants GM-26730 and RR-03960 (to J.H.D.) and GM-53638 (to A.R.B.) and GM-36232 (to B.J.G.). The electromagnet for the Jasco J-500 spectrometer was obtained with a grant from the Research Corp. (to J.H.D.).

* To whom correspondence should be addressed. J.H.D.: Phone (803) 777-7234, Fax (803) 777-9521, E-mail dawson@sc.edu. B.J.G.: Phone (850) 644-8547, Fax (850) 644-8547, E-mail bgaffney@magnet.fsu.edu.

‡ Department of Chemistry and Biochemistry, University of South Carolina.

§ Department of Pharmacology, Vanderbilt University Medical Center.

|| Department of Biological Science, Florida State University.

⊥ School of Medicine, University of South Carolina.

[1] Abbreviations: LOX, lipoxygenase; H(P)ETE, hydro(pero)xyeicosatetraenoic acid; AOS, allene oxide synthase; BLC, bovine liver catalase; TRIS, tris(hydroxymethyl)aminomethane; MES, 2-(*N*-morpholino)ethanesulfonic acid; BCA, bicinchoninic acid; BSA, bovine serum albumin; EDTA, ethylenediaminetetraacetic acid; MCD, magnetic circular dichroism; CD, circular dichroism; EPR, electron paramagnetic resonance.

[2] The truncated form and the intact fusion protein might differ in the efficiency of transfer of the 8R-HPETE substrate to the AOS active site. This remains to be determined and is difficult to study at present due to a limited capability for expression of the intact fusion protein in *E. coli*.

10.1021/bi002121h CCC: $20.00
Published on Web 01/26/2001

growth regulator (*9*, *10*). In coral, the recent discovery of the AOS/LOX fusion protein marks the first characterization of an AOS enzyme in animals (*3*). The coral LOX domain has sequence similarities to other mammalian and plant lipoxygenases; the coral AOS domain has significant sequence homology to catalase, albeit with very low (30%) sequence identity (*3*). It has been shown recently that coral AOS cannot disproportionate hydrogen peroxide like catalases, and catalase cannot convert 8R-HPETE to allene oxide (*4*).

To gain further information about the structure−function relationship for the coral AOS domain, in this study we have probed the heme active site and its environment for the N-terminal domain expressed separately from the C-terminal domain, in *Escherichia coli* (*3*, *4*). For this purpose, we have employed UV−visible absorption, magnetic circular dichroism (MCD), circular dichroism (CD), and electron paramagnetic resonance (EPR) spectroscopic techniques. MCD spectroscopy is used to record the magnetically induced optical activity that correlates with the electronic transitions in the heme group that can be detected with UV−visible absorption spectroscopy (*13*, *14*). Moreover, MCD spectra are difference spectra and consist of considerably more detailed spectral band patterns than the corresponding UV−visible absorption spectra. As a consequence, MCD spectra are much more sensitive than UV−visible absorption spectra to electronic structural changes in the heme that are caused by changes in spin state, coordination number, and the coordinating ligand. Thus, MCD can be used as a powerful "fingerprinting" method for determining the identity of axial ligands in structurally uncharacterized heme proteins by the comparison of their spectral properties with those of known structurally defined heme systems (*13*, *14*). This spectroscopic method has been extensively employed in the past to characterize numerous heme proteins (*13*−*19*). EPR spectroscopy provides information on spin states and can be used as a fingerprint technique for comparison with other proteins containing heme iron. The EPR spectra of low-spin adducts, cyanide adducts for instance, can also be used to compare a protein of unknown proximal ligand to ones where the ligand is known (*20*). The results reported herein reveal that the MCD and EPR spectroscopic properties of various ferric AOS derivatives are very similar to those of the analogous forms of bovine liver catalase (BLC), whose crystal structure has been established at 2.5 Å resolution (*21*). This provides strong evidence for tyrosinate ligation to the AOS heme iron as in BLC (*21*). Interestingly, we have also found that significant differences exist between AOS and BLC in their active site heme environments as revealed by their distinct heme-related CD spectra (with opposite signs) and considerably lower heme ligand binding affinities for AOS than BLC. These differences likely account for, at least in part, the functional difference between the two enzymes.

EXPERIMENTAL PROCEDURES

Materials. All chemicals were purchased from Sigma or Aldrich, except for potassium cyanide, which was obtained from Mallinckrodt, and used as received. The coral AOS domain (∼44 kDa) was overexpressed in *E. coli* and purified ($A_{406}/A_{280} \geq 1.31$ at 4 °C at pH 8.0) as described previously (*3*). For MCD studies, the crystalline suspension of BLC (Sigma, in water containing 0.1% thymol) was extensively dialyzed against water (4 L, ×5) at 4 °C, then against 20 mM potassium phosphate buffer (2 L, pH 7.0), and centrifuged to remove precipitates. For some EPR measurements, BLC containing 0.1% thymol was dialyzed 3 times against 250 volumes of 0.1 M MES, or 0.4 M potassium phosphate, pH 7.0. The BLC samples thus prepared had an $A_{404.5}/A_{280}$ (purity index) value of 0.83−0.87, similar to that reported by Browett and Stillman (*22*). Attempts to further purify BLC using ion exchange chromatography (*23*) in this study did not significantly alter the purity index value.

Preparation of UV−Visible Absorption, MCD/CD, and EPR AOS Samples in the Presence or Absence of Heme Ligands. Stock solutions of purified and concentrated (∼0.71 to ∼0.30 mM) ferric AOS in 50 mM TRIS (pH 8.0) containing 100−150 mM sodium chloride were used after appropriate dilution for a series of UV−visible absorption, MCD/CD, and EPR spectral measurements and for parallel ligand binding studies. Potassium cyanide stock solutions (1 M) were prepared in water by adjusting the pH with phosphoric acid (∼85%) or in 1 M TRIS at pH 8.0. Stock solutions of 1 M sodium azide and 5 M potassium fluoride were prepared in 100 mM potassium phosphate buffer (pH 6.0). Ligands were added to native AOS samples by titration at 4 °C by monitoring with UV−visible absorption spectroscopy until near (80−95%) saturation of the ligand binding was observed. For EPR studies, sodium cyanide (1 M in 1 M TRIS) was added at once to a final concentration of 0.05 M. A stock solution of peracetic acid was prepared by a 20-fold dilution of a 4.1 M commercial sample (Aldrich) into 0.1 M MES buffer and adjusting the pH to 5.5. The peracetic acid solution was pretreated for 30 min with a trace of BLC to remove hydrogen peroxide impurity, as described by Jones and Middlemiss (*24*).

Determination of the Equilibrium Dissociation Constants (K_d Values) for AOS−Ligand Complexes. The K_d values for the AOS−cyanide and AOS−azide complexes were determined by spectrophotometric titrations. Data analysis was done by using a double-reciprocal plot ($1/\Delta A$ vs $1/[L]$) with the equation: $1/\Delta A = K_d/\Delta A_\infty[L] + 1/\Delta A_\infty$, where [L] is the free ligand concentration and ΔA and ΔA_∞ are absorbance changes caused by ligand at $0 < [L] < \infty$ and $[L] = \infty$, respectively. For competitive binding between cyanide and azide to the AOS heme, the apparent equilibrium dissociation constant for cyanide [$K_{d,KCN\ (app)}$] in the presence of azide is expressed as a function of [NaN_3] by using the individual K_d values for cyanide ($K_{d,KCN}$) and azide (K_{d,NaN_3}) as: $K_{d,KCN\ (app)} = K_{d,KCN}\{1 + ([NaN_3]/K_{d,NaN_3})\}$. From this equation, K_{d,NaN_3} can be calculated as: $K_{d,NaN_3} = [NaN_3]/\{(K_{d,KCN\ (app)}/K_{d,KCN}) - 1\}$.

Protein Concentrations. AOS protein concentration was determined in two ways: by colorimetric protein assay (BCA reagent, BSA as standard) and based on the molar extinction coefficient calculated from the amino acid sequence at 280 nm ($\epsilon = 57\ 300\ M^{-1}\ cm^{-1}$). These methods generally agreed to within 15% (e.g., 0.99 and 0.90 mg/mL, respectively, for the BCA and 280 nm methods). BLC concentration was determined based on heme (subunit) using $\epsilon_{404.5} = 100\ mM^{-1}\ cm^{-1}$ for native enzyme at pH 6−7 (*22*).

UV−Visible Absorption, MCD/CD Spectroscopy. UV−visible absorption spectra were recorded using a Varian/Cary 219 spectrophotometer interfaced to an IBM PC for data acquisition. MCD and CD spectra were measured using a

Jasco J500-A spectropolarimeter equipped with a Jasco-MCD-1B electromagnet operated at a field strength of 1.41 T. The J500-A was interfaced to a Gateway 2000 4DX2-66V computer by a Jasco IF-500-2 interface unit. Data acquisition and manipulation have been described elsewhere (*25*). All these spectral measurements were carried out in a 0.2 or 0.5 cm quartz cuvette immediately after sample preparation. Sample temperature was kept at 4.0 ± 0.2 °C with a circulating ethanol/water (50% v/v) bath. UV−visible absorption spectra recorded before and after each MCD/CD measurement were essentially the same.

EPR Spectroscopy. EPR spectra at X-band (~9.2 GHz) were recorded on a Varian E 109 spectrometer equipped with an Oxford Instruments ESR9/10 pumped, gas flow cryostat for liquid helium temperatures and above (*26*). W-band EPR (~94 GHz) spectra were recorded on a Bruker E600 EleXsys heterodyne spectrometer equipped with a TE 011 mode cylindrical resonator, a split-coil superconducting magnet (Magnex) which is capable of linear field sweeps from 0 to 6 T, and an Oxford Instruments automatic helium gas flow cryostat. A current jump method is used to obtain a linear field sweep for W-band measurements (*27*), and specific instrument settings are given in the figure legends. W-band spectra are the average of spectra recorded alternately with increasing or decreasing field sweeps. High-frequency noise was removed from the W-band spectra by application of an exponential filter to the Fourier transform of the field swept spectrum. The *g*-values reported are, from low to high field, g_y, g_x, and g_z for high-spin ferric heme [Blumberg coordinate system (*28*)] and g_z, g_y, and g_x for low-spin heme. The highest and lowest *g*-values were measured at the low-field maximum and high-field minimum, respectively. The middle *g*-value was taken at the point at which the middle spectral line crosses the baseline. The field modulation frequency in recording X-band spectra was 100 kHz, and it was 10 kHz for W-band. Quartz sample tubes were of 0.4 cm outer diameter for X-band and 0.5 mm inner diameter for W-band, and sample sizes were 0.2 and 0.001 mL, respectively.

EPR spectra at both frequencies were obtained with samples of 0.3−0.71 mM AOS in buffer A: 50 mM TRIS, 100−150 mM sodium chloride, and 25% (v/v) glycerol at pH 7.9−8.0, or in buffer B: 0.1 M MES at pH 7.0 (peracetic acid treatment). Samples treated with peracetic acid (1.4 or 14 mM) in buffer B were at either pH 7.0 or pH 5.5, respectively, after the peracetic acid addition, and they were frozen in the spectrometer cryostat within 30−120 s after the addition was made at 4 °C. The EPR spectra of AOS were compared with those of BLC (0.15 mM) in buffer A for native BLC, or in buffer B for peracetic acid treatments.

RESULTS

Heme Content and the Molar Extinction Coefficient of AOS. The heme content of the coral AOS was determined using the pyridine hemochrome assay (*29*). For 2.2 nmol of protein, 1.8 nmol of heme was found. This indicates that the holoenzyme (heme-saturated enzyme) contains 1 mol of heme/mol of enzyme considering that partial heme loss is not unusual for highly purified proteins. Using the calculated molar extinction coefficient at 280 nm based on the amino acid composition of the expressed protein, the millimolar extinction coefficient for the main Soret band at 406 nm was measured as 100 ($n = 3$, values of 98, 99, and 102). Thus, throughout this study, the value of $\epsilon = 100$ mM^{-1} cm^{-1} for the Soret band was used for quantitation of the native ferric AOS at pH values 6−8.

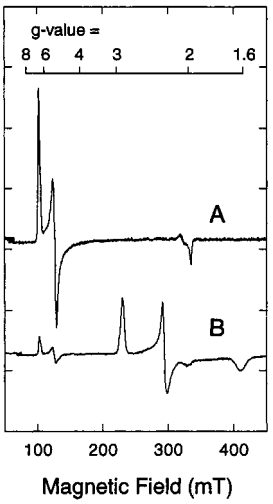

FIGURE 1: The X-band EPR spectra of native allene oxide synthase (AOS) and the cyanide complex. (A) Native AOS (0.71 mM, buffer A, pH 8.0). The EPR signal (9.279 GHz) was recorded at 4 K with modulation amplitude 2 G, microwave power 1.0 mW, time constant 0.128 s, scan time 30 min, and gain 4000. (B) Cyano−AOS (buffer A, pH 8.0). The cyanide complex was prepared by addition of 20 μL of sodium cyanide stock solution (0.5 M) to 180 μL of AOS, both in buffer A, giving final concentrations of 50 mM cyanide and 0.35 mM AOS. The EPR signal (9.273 GHz) was recorded at 8 K with modulation amplitude 10 G, microwave power 1 mW, time constant 1.0 s, scan time 1 h, and gain 8000. The amplitude of spectrum B was scaled approximately to that of spectrum A by multiplying by appropriate ratios of concentration, temperature, modulation amplitude, and gain from each experiment, so that the amplitudes of the two spectra as they appear in the figure can be compared directly.

Characterization of the AOS Spin States. X-band EPR spectra of the coral AOS domain in two forms are shown in Figure 1. The native enzyme as isolated displays a rhombic, high-spin iron ($S = 5/2$) signal with features at g_y-, g_x-, and g_z-values of 6.56(1), 5.22(0), and 2.00(2) ± 0.005 (g_y, g_x) and ±0.001 (g_z), respectively (Figure 1A). Samples of BLC in buffer A gave the same *g*-values, although impurities make additional contributions to BLC EPR signals, especially at low field (*30*). [Based on calculated EPR spectra (*28*), the fraction of high-spin iron giving rise to the low-field impurity signals is approximately 0.l.] At 4 K, the intensity of the X-band EPR spectra of native AOS is linear with the square root of the power of incident microwave radiation to >10 mW, and it drops to 50% of the linear extrapolation (p_{50}) at ~200 mW. The EPR spectrum of AOS in the presence of 50 mM cyanide (pH 8.0) is given in Figure 1B. This spectrum demonstrates that the heme iron in 0.35 mM AOS is predominantly in a low-spin ferric state (cyanide adduct). The EPR signal of cyanide-free AOS is also seen as a minor species under these conditions. The g_z-, g_y-, and g_x-values of the cyanide adduct are 2.85(6), 2.23(8), and 1.60(4) ± 0.005, respectively. These *g*-values are the same as those of the BLC−cyanide complex formed under similar conditions (the BLC EPR spectra, not shown, were recorded for a 0.15 mM BLC sample in 100 mM cyanide, pH 8.0).

The apparent EPR line widths, based on computer simulations (*28*) of the EPR spectra in Figures 1 (simulated spectra

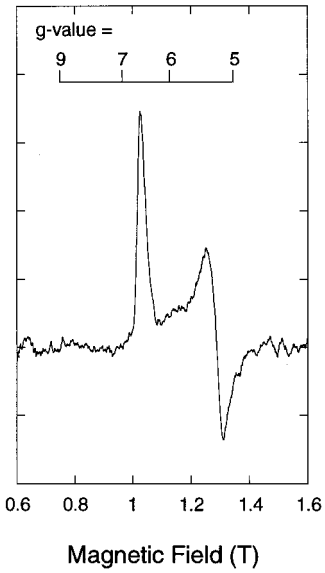

FIGURE 2: Low-field region of the high-frequency (W-band, 94.234 GHz) EPR spectrum of allene oxide synthase (AOS). The spectrum of AOS (0.6 mM, buffer A, pH 8.0) was recorded at 12 K and is the average of scans with increasing and decreasing field sweeps (one each). Instrument settings were as follows: modulation amplitude, 10 G; microwave power, 5 μW; time constant, 0.082 s; and scan rate, 0.74 mT/s.

not shown), arise predominantly from distributions in zero-field splitting values (1A) or *g*-strain (1B) rather than from relaxation. The high-spin AOS spectrum, Figure 1A, is notable in having a $g \sim 2$ (g_z) feature that is as sharp as the lower field features. High- and low-field regions of Figure 1A are fit (fit spectra not shown) better by a Gaussian line width that is constant over the field range than by the theoretical Lorentzian line width that increases over the field range by 1/*g*-factor in a relaxation-determined line shape (*28*). Contributions of zero-field splitting distributions to low-temperature heme EPR line shapes have been examined in detail for hemoglobin and myoglobin (*31*), and similar factors evidently are important contributors to the high-spin iron AOS line shape. The low-spin AOS spectrum (Figure 1B) displays normal line widths that increase as 1/*g*-factor. However, a Gaussian shape fits better than a Lorentzian one, suggesting that the width has a contribution from distributions in-factor (*g*-strain). A small background signal in the region 300−320 mT can be seen in both spectra of Figure 1.

The EPR spectrum of native AOS was also obtained at W-band (94 GHz) (Figure 2). The observed g_y- and g_x-values are not measurably different from those at X-band (9.2 GHz), confirming the expectation that the frequency of the zero-field splitting for the heme iron in AOS is substantially larger than 94 GHz. The zero-field splitting of ferric iron in heme proteins is usually in the range 5−10 cm^{-1} (D = 150−300 GHz) (*28*). The spectrum of BLC at W-band (*32*) is similar to the AOS spectrum, although the low-field peak of the AOS spectrum is the narrower of the two. This may reflect a more homogeneous heme geometry in AOS than in BLC, as the latter is known to contain a small amount of degraded heme (*21*, *22*). The width at half-height of the low-field feature in AOS spectra is 3.4 mT at X-band and 34 mT at W-band. The linear increase in the apparent line width with microwave frequency, together with no shift in *g*-values, is also consistent with a line shape dominated by distributions in zero-field splitting parameters.

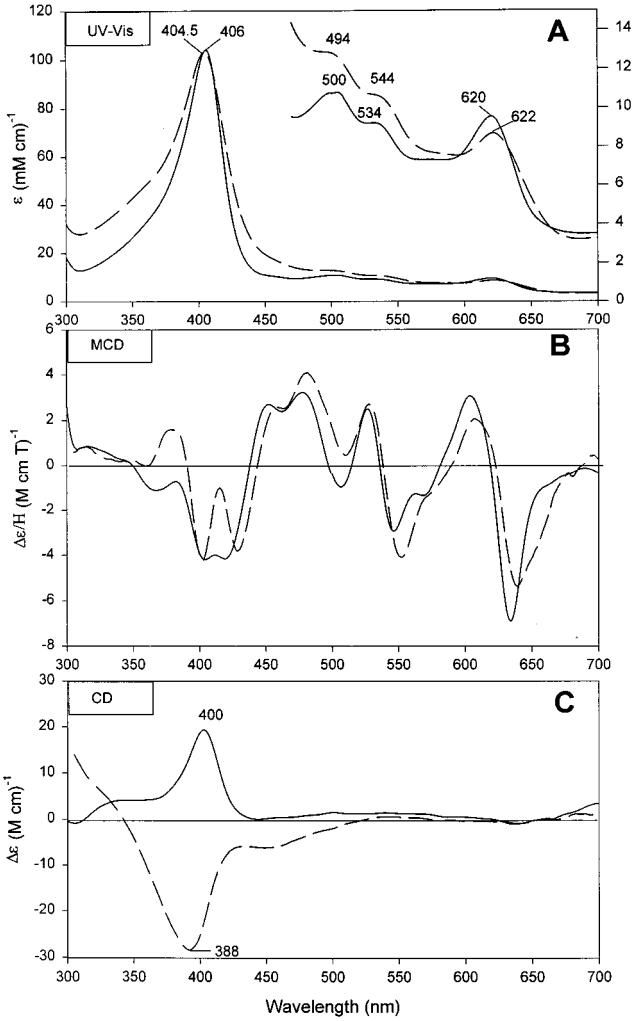

FIGURE 3: UV−visible (UV−Vis) absorption (A), MCD (B), and CD (C) spectra of the native ferric state of allene oxide synthase (AOS) overplotted with the corresponding spectra of bovine liver catalase (BLC). Solid line, AOS (100 μM) at pH 8.0 in 50 mM TRIS buffer, in a 2 mm cuvette; dashed line, BLC (34.7 μM) at pH 6.0 in 50 mM potassium phosphate buffer, in a 5 mm cuvette. Both species were recorded at 4 °C. The spectra of BLC are in good agreement with those reported by Browett and Stillman (*22*).

Heme Ligand Binding Properties of Ferric AOS. Binding of three typical heme ligands, cyanide, azide, and fluoride, to native ferric AOS was examined with UV−visible absorption spectroscopy (Figures 3−5). Among the three ligands, cyanide binds relatively readily (K_d = ∼10 mM at pH values of 7−8 at 4 °C) to AOS accompanying a large, high-spin to low-spin type spectral change (Figure 4A). The binding of azide to AOS is spectrophotometrically less easily detected than that of cyanide, especially in the visible region. Nevertheless, a small spectral change in the Soret region upon addition of azide to AOS (Figure 5A) as well as equilibrium binding experiments for competition between azide and cyanide for the AOS heme confirmed the formation of the AOS−azide complex. More detailed descriptions of the UV−visible absorption spectra of AOS and its ligand adducts will be given below in correlation to their MCD spectra.

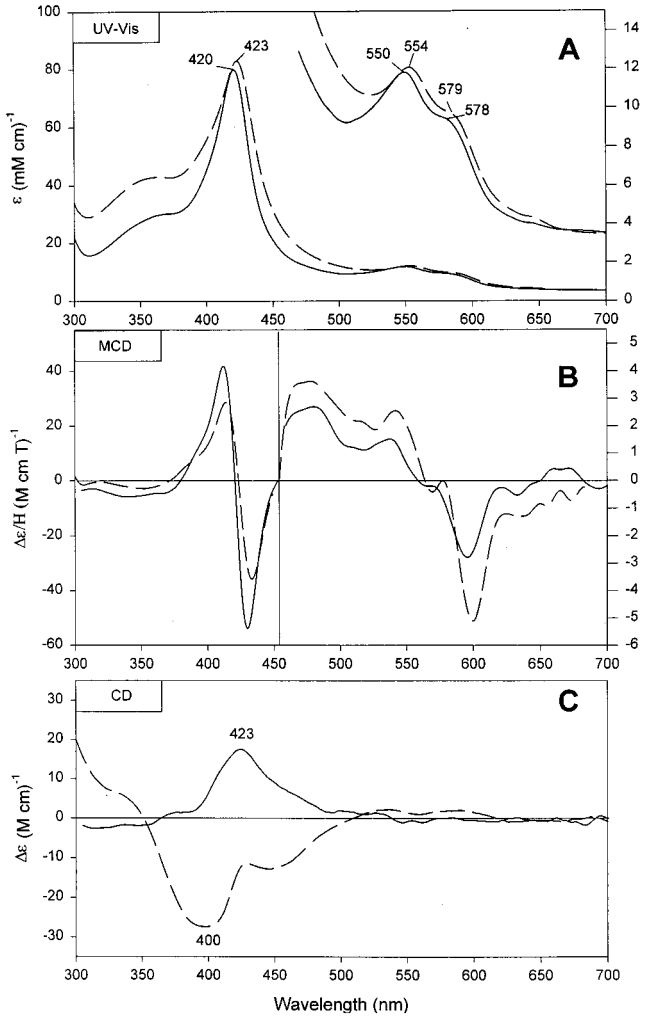

FIGURE 4: UV−visible (UV−Vis) absorption (A), MCD (B), and CD (C) spectra of the ferric cyanide complex of allene oxide synthase (AOS) overplotted with the analogous form of bovine liver catalase (BLC). Solid line, AOS (9.5 μM) at pH 7.0 in 50 mM potassium phosphate buffer, plus 0.2 M potassium cyanide (~95% saturation); dashed line, BLC (21.0 μM) at pH 7.0 in 50 mM potassium phosphate buffer, plus 0.01 M potassium cyanide. In panel B, the left-hand and right-hand side scales are used for the MCD spectra between 300 and 455 nm (vertical line) and between 455 and 700 nm, respectively. The spectra of BLC are in good agreement with those reported by Browett and Stillman (*22*). Both species were recorded at 4 °C in a 5 mm cuvette.

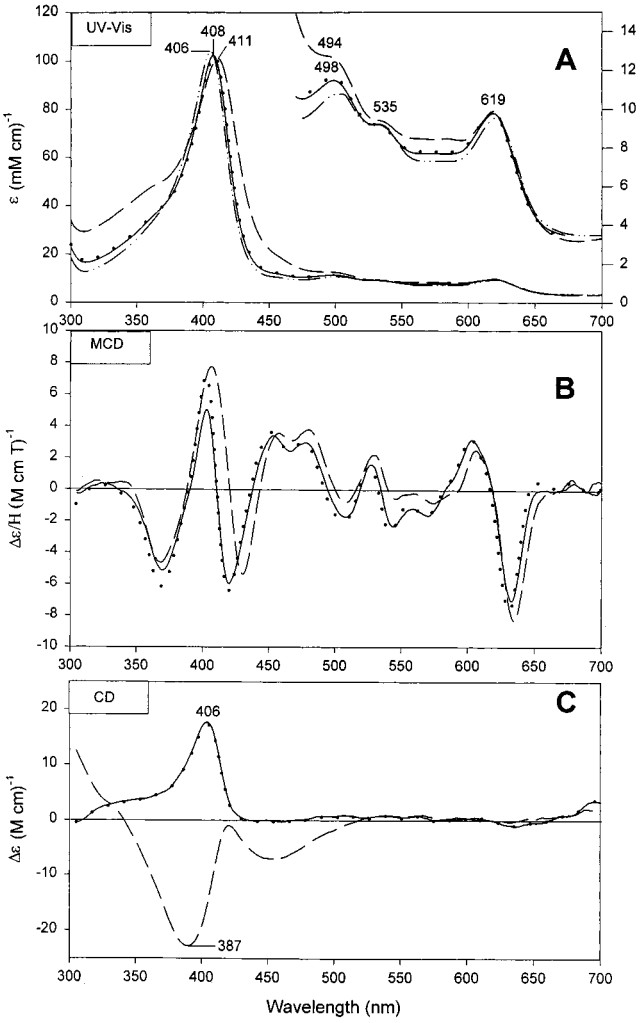

FIGURE 5: UV−visible (UV−Vis) absorption (A), MCD (B), and CD (C) spectra of the ferric azide complex of allene oxide synthase (AOS) overplotted with the analogous form of bovine liver catalase (BLC). Solid line, AOS (20.7 μM) at pH 6.0 in 20 mM potassium phosphate buffer, plus 0.2 M sodium azide (~80% saturation); dashed line, BLC (27.9 μM) at pH 6.0 in 50 mM potassium phosphate buffer, plus 0.2 M sodium azide. The dotted line represents spectra of the fully azide-saturated AOS which is obtained by calculation (see text footnote 3) based on the spectra (solid line) of ~80% azide-saturated AOS (K_d = ~50 mM) (solid line) and azide-free AOS (dot−dot−dash line, not included in panels B and C). The spectra of BLC are in good agreement with those reported by Browett and Stillman (*22*). Both species were recorded at 4 °C in a 5 mm cuvette.

The K_d value for the AOS−azide complex was indirectly determined by competitive binding between azide and cyanide to be ~50 mM at pH 6.0 by the equation: $K_{d,NaN_3} = [NaN_3]/\{(K_{d,KCN(app)}/K_{d,KCN}) - 1\}$ (see Experimental Procedures), where experimental values were $[NaN_3] = 200$ mM, $K_{d,KCN(app)} = \sim 50$ mM, and $K_{d,KCN} = \sim 10$ mM. Direct titration of AOS with azide also yielded a similar K_d value (~60 mM). In the case of fluoride, no detectable spectral changes were observed upon addition of a high concentration (up to 1 M) of KF to native AOS at pH 6−8. Furthermore, the K_d value for the AOS−cyanide complex did not significantly change in the presence of even 1 M fluoride, indicating that the affinity of AOS for fluoride is very low under the conditions used. In comparison, the K_d values for ferric catalase (bovine liver, horse and human erythrocyte) complexes with cyanide, azide, and fluoride under similar conditions have been reported to be 1.5-10 μM, 10-100 μM, and ~20 mM, respectively (*33*, *34*).

UV−Visible Absorption, MCD, and CD Spectral Characteristics of Native AOS and Its Heme Ligand Adducts. UV−visible absorption, MCD, and CD spectra of native ferric AOS and its adducts with the two typical heme ligands cyanide and azide are shown in Figures 3 (native), 4 (ferric-cyanide), and 5 (ferric-azide) in panels A (UV−visible absorption), B (MCD), and C (CD). Corresponding spectra of the BLC species, which were recorded in this study and are in good agreement with those reported previously by Browett and Stillman (*22*), are also plotted for direct comparison. We have not attempted here to give detailed assignments of the MCD spectra because such a study is outside the scope of this work.

Native AOS exhibits four major UV−visible absorption bands in the 300−700 nm region (406, 500, 534, and 619 nm) which closely correspond to those of BLC in both their

positions and intensity (Figure 3A). The ~500 and ~620 nm peaks for the two enzymes are high-spin charge-transfer [porphyrin ($p\pi$) to iron ($d\pi$)] bands (*22*), indicating that native AOS is also high-spin, in agreement with the EPR data (see Figure 1A). The other two absorption bands (406 and 534 nm) arise from $\pi-\pi^*$ transitions in the heme system. Native AOS and BLC exhibit MCD spectra that are remarkably similar to each other in both detailed band pattern and band intensity (Figure 3B). In the Soret region (350−450 nm), BLC shows split MCD troughs (400 and 430 nm) with quite low intensities ($|\Delta\epsilon/H| < 5\ M^{-1}\ T^{-1}\ cm^{-1}$) which are characteristic of other mammalian and bacterial catalases (*35*). This spectral characteristic is also exhibited by AOS, although the resolution of the two troughs is less pronounced for AOS. In the visible region (450−700 nm), the MCD spectral features at ~480 (positive band), ~540 (derivative shape), and ~620 nm (derivative shape) appear at the approximate wavelength positions where the UV−visible absorption bands are seen. It has been shown by Browett and Stillman that the likely contamination by the bile pigment, a heme degradation product, in BLC samples has a negligible effect on the MCD spectra of BLC (*22*). Thus, these MCD data strongly indicate that the electronic structure of the heme group, and therefore the coordination structure, is the same for AOS and BLC.

Upon addition of cyanide (~200 mM) to native AOS, the high-spin marker charge-transfer bands at 619 and ~500 nm disappear in the UV−visible absorption spectrum, and new bands emerge at 550 and 578 nm (Figure 4A). The Soret peak shifts from 406 to 420 nm concomitant with the appearance of a new band at ~370 nm. These spectral changes are indicative of spin state conversion from a high- to a low-spin state, again in agreement with the EPR results (see Figure 1). The resulting absorption spectrum of the AOS−cyanide adduct is almost superimposable to that of the BLC−cyanide complex (Figure 4A). The MCD spectra of the cyanide adducts of AOS and BLC are also very similar to each other (Figure 4B). Both exhibit a simple derivative-shaped [i.e., peak (~410 nm)-crossover (~420 nm)-trough (~435 nm)] spectral pattern in the Soret region and two major peaks (~475 and ~540 nm) and one major trough (~600 nm) in the visible region. As is the case of BLC (*22*), the MCD spectral features between 400 and 450 nm and between 525 and 625 nm (two partially overlapping derivative-shaped bands) appear to be associated with the Soret (420 nm) and the visible (550 and 579 nm) absorption bands (Figure 4A).

Binding of azide to native AOS does not cause a large UV−visible absorption spectral change except that the Soret peak shifts from 406 to 408 nm (Figure 5A) as already mentioned above. To demonstrate the very small spectral change, the spectrum of native AOS (shown in Figure 3A) is also overplotted (dot−dot−dash line) in Figure 5A. Because of the relatively low azide affinity of AOS (K_d = ~50 mM at pH 6.0), we prepared the AOS−azide complex at ~80% azide saturation by adding 200 mM NaN_3 (Figure 5, solid lines). Calculated spectra for fully azide-saturated AOS[3] are shown in Figure 5 by dotted lines. The charge-transfer bands (~500 and ~620 nm) remain even for the fully azide-saturated AOS, indicating that the AOS−azide complex is largely high-spin as is the case of BLC (*22*). In contrast to the small UV−visible absorption spectral change, much larger changes are detected upon azide binding to AOS with MCD spectroscopy in the Soret region (Figure 5B). This clearly demonstrates coordination of azide to the heme iron. The unique double-trough Soret MCD feature in the 390−430 nm region (Figure 3B) completely disappears, and a simple derivative-shaped band pattern is formed in this region upon azide binding to AOS (Figure 5B). Nevertheless, similar UV−visible spectral band assignments and correlation between the MCD features and UV−visible spectral bands can be made for the AOS−azide adduct as have been made above for native AOS. The resulting overall MCD spectrum of the AOS−azide complex is very similar to that of BLC−azide adduct, except that the Soret band for AOS is blue-shifted by ~10 nm as compared with that of BLC. This difference may be attributed, at least in part, to the likely difference in the heme vicinity environmental structure for AOS and BLC (see below for their CD spectra).

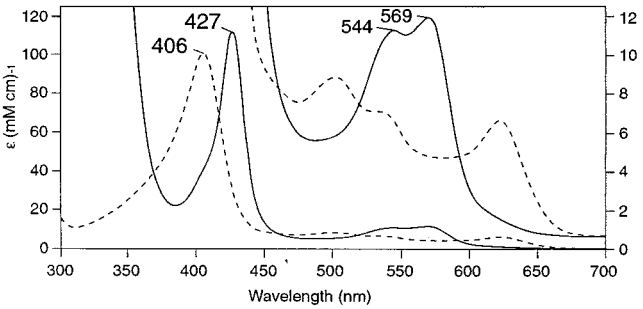

FIGURE 6: UV−visible absorption spectrum of the CO complex of dithionite-reduced allene oxide synthase (AOS). Solid line, the CO complex of dithionite-reduced AOS at pH 7.5 in 50 mM TRIS-HCl buffer recorded at room temperature in a 10 mm cuvette; dashed line, ferric AOS prior to CO treatment. Prior to reduction with dithionite, the solution of ferric AOS was bubbled with CO to facilitate trapping of the ferrous enzyme as the CO complex. Reduction in the absence of CO results in some degradation of the heme chromophore.

Coral AOS and its ligand complexes exhibit CD bands in the Soret region (350−450 nm) (Figures 3−5, panel C) with a positive sign at positions close to their corresponding UV−visible absorption spectral bands (Figures 3−5, panel A). This CD band pattern for AOS is in contrast to that for BLC and its ligand complexes which have negative sign (*22*) with similar intensities. Thus, the CD spectra of AOS and BLC in the Soret region are nearly mirror images of each other. It is also noted that BLC has another, but weaker CD band (a trough) at ~450 nm in its native and ligand complexes while a corresponding CD band for AOS is apparently absent except for its cyanide complex (Figure 4C). The reason for these CD spectral differences has not been examined further in this study. The visible region (450−700 nm) CD spectra of both AOS and BLC were not studied in this work since their intensities are much weaker than those of the Soret region spectra.

UV−Visible Absorption Spectra of the Ferrous States of AOS. The spectral characteristics of the enzyme were examined after reduction with dithionite and treatment with carbon monoxide (Figure 6). Addition of dithionite alone

[3] The observed spectrum for an 80% saturated complex is made up of four parts of the spectrum of the fully saturated complex plus one part of the spectrum of the native protein. Therefore, the calculated spectrum for the fully saturated complex equals 5/4[observed spectrum − (1/5) native spectrum].

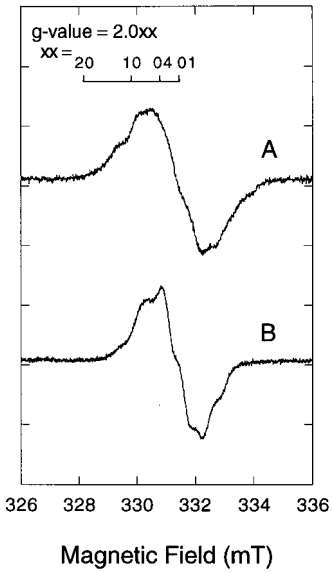

FIGURE 7: X-band EPR signals of radicals formed upon treatment with peracetic acid. Allene oxide synthase (AOS) and bovine liver catalase (BLC) were treated with an excess of peracetic acid (14 mM) and rapidly frozen. The final sample pH values for both enzymes were 5.5. (A) AOS (0.386 mM) and (B) BLC (0.17 mM). The EPR spectra were recorded at 68 K. Instrument settings: modulation amplitude, 1.6 G; microwave power, 1 mW; time constant, 0.25 s; scan time, 30 min; gain, 1.6×10^4.

led to a shift in the main Soret band from 406 to 436 nm, along with a reduction to about two-thirds of the original peak absorbance value (spectrum not shown). The reduced peak absorbance reflects some degradation due to instability of the ferrous enzyme, as is known for catalase itself (*36*). When CO was bubbled through this solution, the 436 nm chromophore shifted to 427 nm with a recovery of the peak absorbance value to about 75% of the original 406 nm signal of the ferric enzyme. This is indicative of CO binding to the remaining ferrous enzyme. To protect the enzyme from the dithionite-induced degradation, the solution of native enzyme was first saturated with CO. When dithionite was then added, the 406 nm band immediately shifted to 427 nm, with a 10% increase in the peak absorbance. CO binding thus helps stabilize the ferrous form of the enzyme yielding the ferrous-CO state that exhibits the Soret peak at 427 nm.

EPR Spectra of AOS After Treatment with Peracetic Acid. Because AOS reacts with its natural substrate, 8R-HPETE, at almost diffusion-controlled rates (*5*), the reaction of the AOS heme center with an oxidant was examined with a potential slow substrate, peracetic acid (*24*). BLC and other catalases are known to react slowly enough with this substrate that Compound I can be trapped by freeze−quench methods (*37*, *38*). The BLC Compound I undergoes further reactions to yield, eventually, a tyrosine radical (*38*, *39*). Treatment of AOS (0.36 mM) with 1.4 mM peracetic acid by manual mixing and quick freezing gave a sample in which the heme EPR signal had been largely replaced by a free radical signal centered at a g'-value of ~2.004. This g-value and the appearance of some hyperfine structure are similar to features of neutral tyrosine radicals in frozen glasses (*40*). When the sample prepared in this manner was stored at 4 °C overnight, and then refrozen for EPR, much of the heme EPR signal (see Figure 1A) was recovered, and some of the radical signal remained. In efforts to obtain a higher yield of the radical signal, AOS was examined further by treatment with a large excess of peracetic acid (0.36 mM AOS; 15 mM oxidant; final pH 5.5), followed by immediate (~30 s) freezing in liquid nitrogen. In this case, most of the high-spin ferric EPR signal was abolished, but the details of the radical EPR signal (Figure 7A) were the same as those obtained with less oxidant. No evidence of an EPR signal with g-values that correspond to those of BLC or bacterial catalase Compound I (g-value range 3.5−2.1) (*37*, *38*) was found in AOS samples trapped 30 s after mixing. For comparison, the EPR spectrum of BLC, treated similarly (BLC, 0.15 mM; oxidant, 14 mM), was also measured (Figure 7B). The spectrum of the BLC radical is also centered at $g \sim 2.004$, and is similar to that reported earlier by Ivancich et al. (*39*).

Line shape calculations (not shown) of the center of the AOS radical signal fit the experimental spectrum well if the hyperfine splittings of the hydrogens are taken as similar to those of neutral tyrosine radicals (*40*), but the AOS spectrum overall is broader than the BLC one. Simulations (not shown) do not easily account for the outer edges of the AOS radical spectrum. There may be an underlying second spectrum in this region, but it is not the g_z feature of high-spin heme because the peracetic acid treatment almost completely abolished the low-field heme signal in the sample reported in Figure 7.

DISCUSSION

The close spectral similarities between the coral AOS domain and BLC as demonstrated in this study using three different spectroscopic techniques (UV−visible absorption, MCD, and EPR) provide strong evidence for tyrosinate ligation to the AOS heme iron as has been established with BLC (*21*). It should be pointed out that none of the particular UV−visible absorption bands (e.g., the ~620 nm charge-transfer band) or MCD spectral features can be directly assigned to the tyrosinate coordination to the heme iron. Rather, the close similarity in the overall AOS MCD spectral band patterns to those of parallel BLC derivatives leads to this conclusion. Based on the crystal structure by Fita and Rossman (*21*) as well as on an MCD study of BLC by Andersson et al. (*35*), it is reasonable to attribute the characteristic UV−visible absorption and MCD spectra of native BLC to the five-coordinate heme having a tyrosinate axial (fifth) ligand with the vacant sixth coordination position (*35*) rather than to a six-coordinate heme having a water molecule as the sixth ligand (*22*). Thus, we conclude that native AOS also has a tyrosinate-ligated five-coordinated ferric heme group. The MCD spectral band pattern similarity for each of the two additional ligation states, ferric-cyanide and ferric-azide, provides further support for tyrosinate ligation to the AOS heme in these states. The indistinguishable EPR spectra for AOS and BLC in their respective native and cyanide-bound states even further strengthen this conclusion.

The AOS domain has been shown to have weak (30%) but significant amino acid sequence homology with catalase including the two corresponding residues (numbering for catalase), His-74 (distal His) and Asn-147 in the distal side of the heme, and the two proximal side residues, Tyr-357 (proximal heme ligand) and Arg-353 (*3*). All these active site amino acids are considered to play important catalytic

or structural roles in catalase function (*21*). Thus, the proximal tyrosinate ligation to the AOS heme iron is not necessarily unexpected. The establishment of the axial ligand identity (tyrosinate) and the coordination structure (five-coordinate) of the heme prosthetic group of coral AOS from its spectroscopic properties is fundamentally important as a first step in understanding the mechanism of action of the enzyme. In addition, the present finding is especially significant and interesting since plant AOS, which catalyzes the same reaction as coral AOS, has been shown to have a cysteinate axial ligand rather than a tyrosinate (*11*).

Furthermore, we have found not only the above spectral similarities but also considerable differences in the Soret region CD spectra (opposite signs) and in the heme ligand affinities between AOS and BLC. Soret (and visible region) CD spectra of heme proteins arise from interactions between the heme and the asymmetric protein environment (*41*). The heme exhibits no optical activity (i.e., no CD signal) in an isolated state because of its high symmetry. Several environmental factors have been shown to influence the sign of Soret CD spectra of heme proteins. Thus, the mirror image Soret CD spectra of AOS and BLC can likely be attributed to differences in the size or hydrophobicity of their active site heme environments (*42*, *43*). The Soret CD sign difference could also be explained as a result of flipping of the heme by 180° about an in-plane axis (*44*).

In addition, the drastically lowered affinity of AOS for heme ligands (cyanide, azide, fluoride) as compared with that of catalase by a factor of ≥ 500 could also be attributed to probable differences in the active site heme environments of the two enzymes. Since these ligands are relatively small and ligate to the heme iron in their anionic form, the polarity of the active site environment or the availability of a residue(s) that would stabilize the heme iron-bound ligands such as through a hydrogen bond would significantly influence the ligand affinity of the AOS domain. Steric factors at the distal side vicinity of the heme group might also influence the ligand affinity of the heme. Such cases have been demonstrated in site-directed mutagenesis studies of myoglobin (*45*). Furthermore, unlike BLC (*36*, *46*), AOS is relatively readily reducible with sodium dithionite, indicating that accessibility to dithionite anion is considerably different for the hemes of the two enzymes.

These differences between coral AOS and BLC are most likely related to the recent finding that, despite the significant amino acid sequence homology to catalase, the AOS domain completely lacks catalase-like activity (on H_2O_2) and, conversely, catalase is incapable of converting 8R-HPETE to allene oxide (*4*). Thus, AOS and BLC are among the interesting examples of conserved primary structure but different function. However, from detailed comparison of the sequences of AOS and BLC, and with respect to the X-ray structure of the latter, there appear to be significant differences between AOS and catalase in regions that interact with the side chains of the heme group. In particular, residues corresponding to BLC β-strands-3 and -4, α-helix-3, and the loop before helix-9 are not similar in the two proteins. In addition, the separate AOS domain ends at residue 373 (about 381 in BLC) and thus is missing more than 100 residues at the C-terminus of BLC. The carboxy-terminal region missing in AOS would include much of the "wrapping domain" and the entire fourth domain of the BLC structure. In BLC, the fourth domain provides many of the residues forming the channel leading to the heme (*21*).

Even though plant AOS utilizes the thiolate-ligated heme prosthetic group and the enzyme belongs to a cytochrome P450 gene family (*4*), the reaction it catalyzes is not a typical P450 reaction; plant AOS does not require either a reductant [NAD(P)H] or molecular oxygen. According to a proposed mechanism (*47*), ferric AOS reacts with fatty acid hydroperoxide to generate initially an alkoxy radical and oxo−ferryl [O═Fe(IV)] heme by homolytically cleaving the O−O bond of the peroxide. This reaction is distinct from that of heme peroxidases which carry out heterolytic O−O bond cleavage of hydroperoxides (*48*). It is proposed that the alkoxy radical species thus produced by AOS rearranges to an epoxide and a carbon radical, the latter of which is subsequently oxidized by the oxo−ferryl heme of the enzyme to generate, upon β-proton elimination, a C═C bond adjacent to the epoxide group and ferric heme (resting enzyme) plus water. Thus, the overall reaction catalyzed by AOS is dehydration of a fatty acid hydroperoxide. It is interesting to note that even though plant and coral AOS belong to completely different families of protein, both enzymes catalyze the same reaction by utilizing anionic axial heme ligands, cysteinate and tyrosinate, respectively, rather than histidine which is more common to heme peroxidases.

At low concentrations (0.5−10 μM), mammalian catalases are known to be oxidized by peracetic acid (30−50 μM) or alkyl hydroperoxides ($\sim$100 μM) to form an oxo−ferryl porphyrin π-cation radical (Compound I) as judged by UV−visible absorption spectroscopy (*22*, *49*, *50*). The same derivative has also been observed with EPR spectroscopy for bacterial (*Micrococcus luteus*) catalase (0.5 mM) following addition of peracetic acid (3 mM) (*37*). However, addition of a large excess amount of peracetic acid (10−25 mM) to BLC (0.01−0.5 mM) has been shown to generate a Compound II (oxo−ferryl)-type derivative as judged by UV−visible absorption spectroscopy (*49*); a free radical species has also been detected with EPR spectroscopy (*39*). Formation of the BLC radical has been examined by others by rapid mixing−freeze quench at 10 °C and pH 5.6 using (as final concentrations) $\sim$0.175 mM catalase and $\sim$13 mM peracetic acid (*38*). Under these conditions, the lifetime of the BLC Compound I EPR signal was less than 1 s, while the intensity of a tyrosine radical signal increased for at least 15 s. The present study has demonstrated that the coral AOS domain ($\sim$0.39 mM) reacts with a 4-fold or greater excess of peracetic acid to produce a free radical with EPR spectral properties that are close to those of a BLC radical obtained under similar conditions. The latter has been attributed to a tyrosine radical (*39*). The readily saturated EPR signal for the radical species of AOS (this study) as well as for BLC (*39*) suggests that the radical is located on a tyrosine group other than the heme axial ligand for both enzymes. BLAST alignment of AOS and BLC (*3*) reveals three tyrosines in the regions of homology, besides the one in the heme binding region. These are at positions in AOS (BLC): 193 (214), 209 (230), and 269 (324). The BLC tyrosine at 214 has been considered as the radical site in discussions of electron tunneling between iron and the NAD(P)H site (*48*).

Formation of a tyrosine radical in AOS may result from similar fast reactions that begin with formation of Compound I. If so, formation of an AOS oxo−ferryl species would be

significant since this species is proposed as an intermediate in the AOS-catalyzed synthesis of allene oxide (*47*). The tyrosine radical in catalase has been the subject of discussion of long-range electron-transfer pathways involving single electron redox reactions that protect catalases from self-destruction by Compound I (*51*). Further studies are in progress to elucidate the mechanism of action and the molecular structure−function relationship of coral AOS, a unique heme enzyme that is spectrally similar to, but functionally distinct from, catalase.

ACKNOWLEDGMENT

We thank William Boeglin for help in preparation of the AOS domain, and Drs. Edmund W. Svastits and John J. Rux for developing the computer-based spectroscopic data-handling system for the MCD/CD.

REFERENCES

1. Brash, A. R., Baertschi, S. W., Ingram, C. D., and Harris, T. M. (1987) *J. Biol. Chem. 262*, 15829−15839.
2. Corey, E. J., d'Alarcao, M., Matsuda, S. P. T., and Landsbury, P. T. J. (1987) *J. Am. Chem. Soc. 109*, 289−290.
3. Koljak, R., Boutand, O., Shieh, B.-H., Samuel, N., and Brash, A. R. (1997) *Science 277*, 1994−1996.
4. Boutaud, O., and Brash, A. R. (1999) *J. Biol. Chem. 274*, 33764−33770.
5. Varvas, K., Järving, I., Koljak, R., Valmsen, K., Brash, A. R., and Samel, N. (1999) *J. Biol. Chem. 274*, 9923−9929.
6. Kikuchi, H., Tsukitani, Y., Iguchi, K., and Yamada, Y. (1982) *Tetrahedron Lett. 23*, 5171−5174.
7. Baker, B. J., Okuda, R. K., Yu, T. K., and Scheuer, P. J. (1991) *J. Am. Chem. Soc. 107*, 2976−2977.
8. Hamberg, M. (1989) *J. Am. Oil Chem. Soc. 66*, 1445−1449.
9. Hamberg, M., and Gardner, H. W. (1992) *Biochim. Biophys. Acta 1165*, 1−18.
10. Grechkin, A. (1998) *Prog. Lipid Res. 37*, 317−352.
11. Song, W. C., and Brash, A. R. (1991) *Science 253*, 781−784.
12. Blée, E. (1998) *Prog. Lipid Res. 37*, 33−77.
13. Dawson, J. H., and Dooley, D. M. (1989) in *Iron Porphyrins, Part III* (Lever, A. B. P., and Gray, H. B., Eds.) pp 1−87, VCH Publishers, New York.
14. Cheek, J., and Dawson, J. H. (2000) in *The Porphyrin Handbook* (Kadish, K. M., Smith, K. M., and Guilard, R., Eds.) Vol. 7, pp 339−369, Academic Press, New York.
15. Dawson, J. H., and Sono, M. (1987) *Chem. Rev. 87*, 1255−1276.
16. Sono, M., Stuehr, D. J., Ikeda-Saito, M., and Dawson, J. H. (1995) *J. Biol. Chem. 270*, 19943−19948.
17. Roach, M. P., Chen, Y. P., Woodin, S. A., Lincoln, D. E., Lovell, C. R., and Dawson, J. H. (1997) *Biochemistry 36*, 2197−2202.
18. Alberta, J. A., Andersson, L. A., and Dawson, J. H. (1989) *J. Biol. Chem. 264*, 20467−20473.
19. Burstyn, J. N., Yu, A. E., Dierks, E. A., Hawkins, B. K., and Dawson, J. H. (1995) *Biochemistry 34*, 5896−5903.
20. Peisach, J. (1998) in *Foundations of Modern EPR* (Eaton, G. R., Eaton, S. S., and Salikov, K. M., Eds.) pp 346−360, World Scientific, Singapore.
21. Fita, I., and Rossmann, M. G. (1985) *J. Mol. Biol. 185*, 21−37.
22. Browett, W. R., and Stillman, M. J. (1979) *Biochim. Biophys. Acta 577*, 291−306.
23. Morikofer-Zwez, S., Cantz, M., Kaufmann, H., von Wartburg, J. P., and Aebi, H. (1969) *Eur. J. Biochem. 1*, 49−57.
24. Jones, P., and Middlemiss, D. N. (1972) *Biochem. J. 130*, 411−415.
25. Huff, A. M., Chang, C. K., Cooper, D. K., Smith, K. M., and Dawson, J. H. (1993) *Inorg. Chem. 32*, 1460−1466.
26. Gaffney, B. J., Mavrophilipos, D. V., and Doctor, K. S. (1993) *Biophys. J. 64*, 773−783.
27. *EleXsys User's Manual*, Bruker Instruments, Manning Park, MA.
28. Gaffney, B. J., and Silverstone, H. J. (1993) *Biol. Magn. Reson. 13*, 1−57.
29. Paul, K. G., Theorell, H., and Åkeson, Å. (1953) *Acta Chem. Scand. 7*, 1284−1287.
30. Peisach, J., Blumberg, W. E., Ogawa, S., and Rachmilewitz, E. A. (1971) *J. Biol. Chem. 246*, 3342−3355.
31. Fiamingo, F. G., Brill, A. S., Hampton, D. A., and Thorkildsen (1989) *Biophys. J. 55*, 67−77.
32. Gaffney, B. J., Maguire, B. C., Weber, R. T., and Maresch, G. G. (1999) *Appl. Magn. Reson. 16*, 207−221.
33. Ogura, Y., Tonomura, Y., Hino, S., and Tamiya, H. (1950) *J. Biochem. 37*, 153−177.
34. Chance, B. (1952) *J. Biol. Chem. 194*, 471−496.
35. Andersson, L. A., Johnson, A. K., Simms, M. D., and Willingham, T. R. (1995) *FEBS Lett. 370*, 97−100.
36. Schonbaum, G. R., and Chance, B. (1976) in *The Enzymes (Second Edition)* (Boyer, P. D., Ed.) Vol. XIII, pp 363−408, Academic Press, New York.
37. Benecky, M. P., Frew, J. E., Scowen, N., Jones, P., and Hoffman, B. M. (1993) *Biochemistry 32*, 11929−11933.
38. Ivancich, A., Jouve, H. M., Sartor, B., and Gaillard, J. (1997) *Biochemistry 36*, 9356−9364.
39. Ivancich, A., Jouve, H. M., and Gaillard, J. (1996) *J. Am. Chem. Soc. 118*, 12852−12853.
40. Hulsebosch, R. J., van den Brink, J. S., Nieuwenhuis, S. A. M., Gast, P., Raap, J., Lugtenburg, J., and Hoff, A. J. (1997) *J. Am. Chem. Soc. 119*, 8083−8094.
41. Hsu, M.-C., and Woody, R. W. (1971) *J. Am. Chem. Soc. 93*, 3515−3525.
42. Ollis, D. L., Appleby, A. A., Colman, P. M., Cutten, A. E., Guss, J. M., Venkatappa, M. P., and Freeman, H. (1983) *Austr. J. Chem. 36*, 451−468.
43. Myer, Y. P., and Pande, A. (1978) in *The Porphyrins* (Dolphin, D., Ed.) Vol. III, pp 271−322, Academic Press, New York.
44. Aojula, H. S., Wilson, M. T., Moore, G. R., and Williamson, D. J. (1983) *Biochem. J. 250*, 853−858.
45. Brancaccia, A., Cutruzzola, F., Allocatelli, C. T., Brunori, M., Smerdon, S. J., Wilkinson, A. J., Dou, Y., Keenan, D., Ikeda-Saito, M., Brantley, R. E., and Olson, J. S. (1994) *J. Biol. Chem. 269*, 13843−13853.
46. Keilin, D., and Hartree, E. F. (1937) *Proc. R. Soc. London, Ser. B. 121*, 173.
47. Mansuy, D., and Renaud, J.-P. (1995) in *Cytochrome P450: Structure, Mechanism, and Biochemistry, Second Edition* (Ortiz de Montellano, P. R., Ed.) pp 537−573, Plenum Press, New York.
48. Poulos, T. L. (1987) *Adv. Inorg. Biochem. 7*, 1−36.
49. Browett, W. R., and Stillman, M. J. (1980) *Biochim. Biophys. Acta 623*, 21−31.
50. Palcic, M. M., and Dunford, H. B. (1980) *J. Biol. Chem. 255*, 6128−6132.
51. Olson, L. P., and Bruice, T. C. (1995) *Biochemistry 34*, 7335−7347.

BI002121H